

# Automatic landslide mapping from satellite imagery with a topography-driven thresholding algorithm

Massimiliano Alvioli<sup>§</sup>, Alessandro C. Mondini, Federica Fiorucci, Mauro Cardinali, Ivan Marchesini

Istituto di Ricerca per la Protezione Idrogeologica,  
Consiglio Nazionale delle Ricerche  
via Madonna Alta, 126 I-06128, Perugia, Italy  
<sup>§</sup> massimiliano.alvioli@irpi.cnr.it

**Abstract—** We present an improvement of image classification by “thresholding”, using topographic information to determine multiple thresholds. We devised a two-steps procedure for automatic classification into landslide or no landslide categories of a change-detection map obtained from satellite imagery. Requirements of the proposed procedure are knowledge of the occurrence of a landslide event, availability of a pre- and post-event pseudo-stereo image pair and a digital elevation model. The novel feature of the approach is represented by the use of slope units as topographic-aware subsets of the scene within which we apply a multiple thresholding method to classify a landslide class membership tuned on the sole landslide spectral response. The method is fully automatic after site-dependent operations, required only once, are performed, and exhibits improved classification performance with limited training requirements. Our automatic procedure is a step forward towards systematic acquisition of landslide events and real-time landslide mapping from satellite imagery.

## I. INTRODUCTION

The most effective source of information describing a landslide event extension and magnitude in a given region is an event landslide inventory map (eLIM). An eLIM is a key input to derive landslide hazard and risk maps, and its preparation require effective monitoring and fast, cost-efficient mapping tools. More in general, despite their importance, landslide inventory maps cover a limited extension of the landslide-prone areas across the global landmass [1,2].

Landslide inventory maps are best prepared by visual interpretation of stereoscopic aerial images [3]. In the last two decades the images captured by high resolution and very high resolution optical satellites [1,4,5], and synthetic aperture radar [4,6], are becoming a viable replacement of aerial photographs, encouraging research efforts in the direction of developing automatic and semi-automatic classification algorithms to

distinguish different land covers, including vegetation, urban areas, water bodies and landslides. Use of LiDAR data for automatic landslide mapping is beyond the scope of this work, mainly because it is not suitable for use within the approach described here, and will not be discussed.

Automatic and semi-automatic landslide mapping require image classification methods, including supervised and unsupervised clustering [7,8], and index thresholding [5,9]. Supervised classification calls for a manual training process which can result difficult and time consuming. Reducing the time and the overall effort required to prepare an eLIM, while increasing the level of automation of the mapping procedure, are key issues to obtain a reliable estimate of the extent and magnitude of landslide events on a routinely basis.

In this work, we focus on a classification method which assigns individual pixels to the generic bare soil class, with a spectral fingerprint corresponding to event landslides [10]. We use a Bayesian-based maximum likelihood (ML) approach to assign each pixel either to the “landslide” or “no landslide” land cover classes by thresholding, the simplest existing decision rule. The procedure requires to single out a numerical value (threshold), among all the values in the image, and to assign the pixels values above (or below) the threshold to a particular class [11]. We used thresholding to classify a change detection (CD) function, obtained from a combination of widely used change detection indices tuned on landslide spectral response. In particular, we devised a multi-threshold approach that takes advantage of the topographic information contained in a slope unit (SU) subdivision of the area under investigation [12,13,14,15]. Using a custom classification threshold within each slope unit allows to overcome limitations posed by the different geometric conditions, dictated by the combination of satellite point of view, sun position, slope orientation and

78 inclination. Such conditions can be considered homogeneous  
 79 within typical individual SUs, while they pose limitations when  
 80 the CD function values are classified using a single threshold. A  
 81 large number of false negatives and false positives are inherently  
 82 introduced by a single threshold. On the other hand,  
 83 misclassifications may be strongly reduced using multiple  
 84 thresholds.

85 II. METHOD AND RESULTS

86 Our method to automatically identify the pixels belonging to  
 87 the landslide land cover class relies on the concept of a CD  
 88 function, denoted here and in Ref. [5] as  $g_{ls}$  ("ls" stands for  
 89 "landslides"), obtained with a simplified ML classifier. Figure 1  
 90 summarizes the method developed in Ref. [5], illustrating the two  
 91 basic steps, updated in this work.

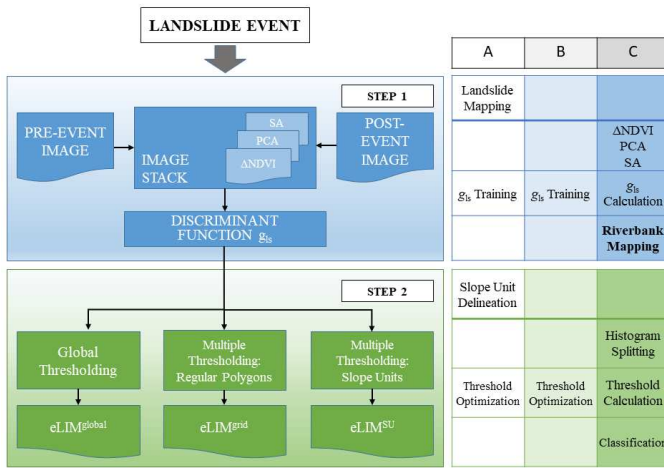


Figure 1. The algorithm proposed in Ref. [5], and updated in this work, applied upon knowledge of the occurrence of a landslide event. Step 1: calculation of the discriminant function; step 2: three different classification possibilities by index thresholding, resulting in three different eLIMs (cf. Section II). The table describes the level of automation of the individual operations involved in each of the two steps. A: one-time, site-dependent operations; B: operations that can be optionally performed again in a new study area; C: fully automatic operations, to which we added "Riverbank Mapping" in this work, with respect to Ref. [5].

92 In the first step, we define the function  $g_{ls}$  whose values  
 93 represent the ML distance of each pixel from the landslide class,  
 94 providing a pixel-by-pixel measure of the presence or absence of  
 95 new landslides. The  $g_{ls}$  function is obtained measuring changes  
 96 occurred between a pre- and a post-event image, using three  
 97 different metrics: changes of NDVI [16], Spectral Angle (SA)  
 98 [17,18,19] and Principal Component Analysis (PCA) [18]. The  
 99 three metrics were combined in a single image stack of changes  
 100 for the analysis.

101 In the second step, a map is generated by evaluating the  $g_{ls}$   
 102 function in each pixel of the study area. Then the  $g_{ls}$  map pixels  
 103 are classified as "landslide" or "no landslide", either by: (i)  
 104 thresholding the  $g_{ls}$  values, i.e., selecting as landslides the pixels  
 105 with  $g_{ls}$  values larger than a single threshold value over the whole  
 106 study area; (ii) using multiple threshold values, within square and  
 107 rectangular subsets of the  $g_{ls}$  map; (iii) as in (ii), but replacing  
 108 regular subsets with irregular SU polygons, thus introducing local  
 109 geomorphological information.

110 In the first step, the innovative feature is represented by the  
 111 fact that we only aim at defining the landslide class, thus we only  
 112 need to train the procedure once. In the test case of Ref. [5], the  
 113 calibration area was selected in only one (big) landslide, for a  
 114 total of 421 pixels (about 10,000 m<sup>2</sup> out of about 1,000 km<sup>2</sup>) in  
 115 the stack of changes.

116 In the second step, the core innovation of the procedure is the  
 117 application of thresholding  $g_{ls}$  values within a large number of  
 118 subsets of the study area, singled out either with and without a  
 119 topographic information. Existing thresholding approaches use a  
 120 single threshold, necessarily reducing accuracy, while SU  
 121 provide local topography information and allows to find local  
 122 custom thresholds.

123 The proposed method was tested in an area of about 1,000 m<sup>2</sup>  
 124 in Myanmar, where torrential rainfall triggered extensive  
 125 landslides in 2015, including the massive Tonzang landslide and  
 126 the large number of fatalities [21].

127 Figure 2 shows histograms of the values for the CD  
 128 discriminant function  $g_{ls}$ . A distinctive feature of the global  
 129 histogram, Fig. 2(a), is a bi-modal behavior, characterized by a  
 130 small peak around  $g_{ls} = 0$ , overwhelmed by a broad peak  
 131 containing the vast majority of pixels with spectral properties  
 132 dissimilar from the landslide ones. The two peaks (modes) are  
 133 separated by a well-defined local minimum, occurring at some  $g_{ls}$   
 134 value denoted as  $M$ . The first approximation to a binary  
 135 classification of the  $g_{ls}$  values is to flag as "landslide" the pixels  
 136 with  $M < g_{ls} < 0$ , and to flag as "no-landslide" the remaining  
 137 pixels.

138 The next approximation we discuss consists in tracing a grid  
 139 onto the  $g_{ls}$  map, calculate a histogram of the values of  $g_{ls}$  for  
 140 each rectangular polygon singled out by the grid (cf. Fig. 2(b)-  
 141 (e)), and process the histogram with the automatic, non-  
 142 parametric mode detection software of Ref. [18], implemented as  
 143 standalone program. Depending on the number and values of the  
 144 separations between different modes found by the software, we  
 145 developed an algorithm to determine custom thresholds to be  
 146 applied within the single polygons we introduced.

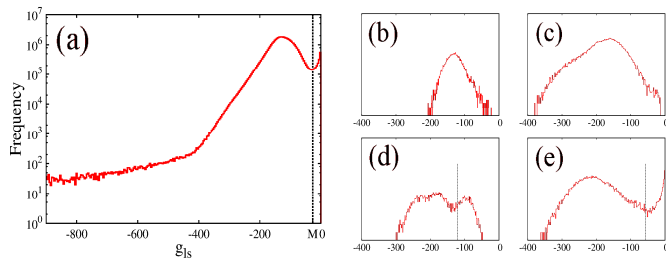


Figure 2. (a): histogram of the  $g_{ls}$  function values over the whole study area. (b-d): four sample histograms of the  $g_{ls}$  values, corresponding to four individual slope units. The vertical lines represent the divide between different modes, if any. The mode located right from the divide may be due (e), or may not be due (d), to pixels with spectral behavior very similar to pixels known to be within the landslides selected for the training procedure, by construction of  $g_{ls}$ .

147

148 The third and last approximation is to replace the rectangular  
 149 polygons with topography-aware slope units. SU were delineated  
 150 using the automatic software of Ref. [12], using a portion of  
 151 ASTER digital elevation model, and are shown in Fig. 3 for the  
 152 calibration study area (about  $\frac{1}{4}$  in size of the whole area). The  
 153 number and size of SU were chosen maximizing agreement of  
 154 the automatic classification with an eLIM prepared by expert  
 155 geomorphologists, by photo-interpretation, in a calibration  
 156 region. The method was then extended to a different, and wider,  
 157 validation region. Visual interpretation and  $g_{ls}$  analysis were  
 158 performed on a 5m x 5m RapidEye stereo-pair.

159

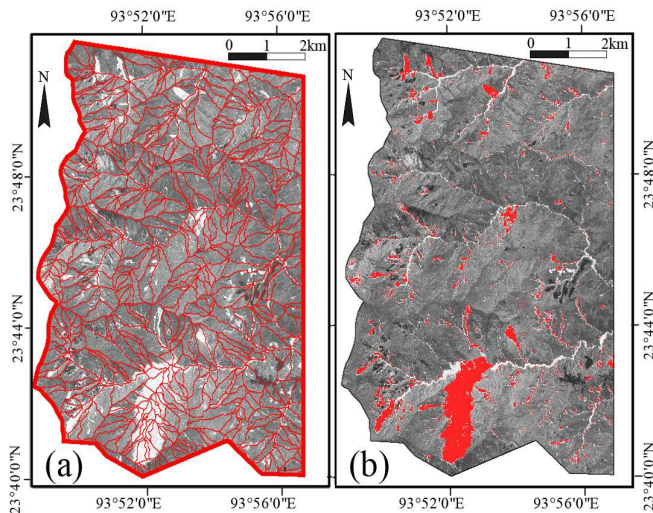


Figure 3. (a): the SU subdivision of the calibration area, in the calibration subset of our test area located in Myanmar (see Ref. [5] for details). (b): red pixels denote the automatically-mapped landslide inventory,  $eLIM^{SU}$  (cf. Fig. 1), obtained with multiple thresholds within the SU polygons shown in (a).

160

161 In this work, we added an additional level of automation with  
 162 respect to the work in Ref. [5]. The comparison between  
 163 automatic and expert mapping was performed everywhere but on  
 164 pixels corresponding to rivers. We automated riverbanks  
 165 mapping using a pixel-based method [10,23], thus making the  
 166 overall method fully automatic after site-dependent operations,  
 167 required only once, are performed. Such operations are listed in  
 168 Fig. 1.

169 We report results of the three different approximations (also  
 170 reported in Ref. [5]), expressed in terms of an error index  $E_l$ , first  
 171 introduced in Ref. [12] and recently employed as a benchmark  
 172 for selecting optimal requirements of images from remote  
 173 sensing for landslide mapping [22]. Results for “grid” and “SU”  
 174 are obtained with a number of polygons that minimizes  $E_l$  in both  
 175 cases. Results are listed in Table I. The percentage gain of multi-  
 176 thresholding with respect to the “global”, single-threshold results,  
 177 are calculated as  $(E_l^{SU} - E_l^{global})/E_l^{global}$ , in the SU case, and  
 178 correspond to 8.1% in training and 4.8% in validation.

179 Eventually, we replaced riverbanks mapped by visual  
 180 interpretation with a riverbank layer mapped automatically and  
 181 calculated  $E_l$  in the training area using the new layer; results are  
 182 listed in Table I as well. The percentage gain using SUs (7.7%)  
 183 is comparable to the results obtained with visual mapping of  
 184 riverbanks (8.1%).

Table I. Numerical results from the comparison of eLIMs obtained with global thresholding and with grid-based and SU-based multi-threshold presented in this work and Ref. [5].

Riverbanks mapping		Training			Validation		
		$E_l$	Gain		$E_l$	Gain	
Visual	$E_l$	0.369	0.344	0.339	0.512	0.510	0.487
	Gain	-	6.7%	8.1%	-	0.4%	4.8%
Automatic	$E_l$	0.401	-	0.370	-	-	-
	Gain	-	-	7.7%	-	-	-

186

### III. DISCUSSION AND CONCLUSIONS

187 The topography-driven, multi-threshold approach to  
 188 landslide mapping from satellite imagery proposed in Ref. [5],  
 189 and updated in this work, presents several advantages.

190 The numerical results of the comparison of the automatic  
 191 mapping procedure with the ground-truth of an eLIM prepared  
 192 by visual interpretation (Table I) reveal that the topographic-  
 193 aware subdivision of the territory allows for a better  
 194 classification performance both than thresholding applied  
 195 globally, or within a topographic-blind subdivision. This is  
 196 particularly true in the validation area, where the grid-based  
 197 method shows little gain (0.4%) with respect to the global  
 198 thresholding method.

In second place, we substantially simplified image preparation with respect to existing land cover classification methods using remote sensing. Considering the only “landslide” class reduces the time and effort needed to train the algorithm to distinguish the spectral response of landslides.

In third place, once the preliminary steps of SU delineation,  $g_{ls}$  training and calibration of thresholds are performed, the procedure is fully automatic, including the detection of riverbanks, left out of our previous work [5]. Class assignment is automatic and it does not require a-posteriori identification of the different classes. Figure 1 contains a table describing the different levels of automation of the various actions required to achieve multi-threshold classification.

In preparing the  $g_{ls}$  function map, we combined three indices embodying both radiometric ( $\Delta NDVI$  and SA) and geometric (PCA) information contained in satellite images, to account for the heterogeneity showed by the spectral response of landslides [19,24]. Further developments may include different indices, in the discriminant function preparation, or additional topographic drivers [25]. The method can be used on a routinely basis, and run whenever the occurrence of a new landslide event is otherwise detected with specialized methods [6,23].

In conclusion, we argue that the improved performance and limited training requirements of the classification procedure represent a step forward towards an automatic, reliable real-time landslide mapping from satellite imagery.

REFERENCES

[1] Guzzetti, F., A.C. Mondini, M. Cardinali, F. Fiorucci, M. Santangelo, K. T. Chang, 2012. “Landslide inventory maps: New tools for an old problem”. *Earth-Science Reviews* 112(12), 42-66.

[2] Marchesini, I., F. Ardizzone, M. Alvioli, M. Rossi, F. Guzzetti, 2014. “Non-susceptible landslide areas in Italy and in the Mediterranean region”. *Natural Hazards and Earth System Sciences* 14, 2215-2231.

[3] Fiorucci, F., M. Cardinali, R. Carlà, M. Rossi, A. Mondini, L. Santurri, F. Ardizzone, F. Guzzetti, (2011). “Seasonal landslide mapping and estimation of landslide mobilization rates using aerial and satellite images”. *Geomorphology* 129(12), 59-70.

[4] Casagli, N., W. Frodella, S. Morelli, V. Tofani, A. Ciampalini, E. Intrieri, F. Raspini, G. Rossi, L. Tanteri, P. Lu, 2017. “Spaceborne, UAV and ground-based remote sensing techniques for landslide mapping, monitoring and early warning”. *Geoenvironmental Disasters*. 4(1):9.

[5] Alvioli, M., A. C. Mondini, F. Fiorucci, M. Cardinali, I. Marchesini, 2018. “Topography-driven satellite imagery analysis for landslide mapping”. *Geomatics, Natural Hazards & Risk* 9(1), 544-567.

[6] Mondini, A.C., 2017. “Measures of spatial autocorrelation changes in multitemporal SAR images for event landslides detection”. *Remote Sensing* 9(6).

[7] Borghuis, A.M., K. Chang, H. Y. Lee, 2007. “Comparison between automated and manual mapping of typhoon triggered landslides from spot 5 imagery”. *International Journal of Remote Sensing* 28(8), 1843-1856.

[8] Martha, T.R., N. Kerle, C. J. van Westen, V. Jetten, K. V. Kumar, 2011. “Segment optimization and data-driven thresholding for knowledge-based

landslide detection by object-based image analysis”. *IEEE Transactions on Geoscience and Remote Sensing*. 49(12), 4928-4943.

[9] Rosin, P.L., J. Hervás, 2005. “Remote sensing image thresholding methods for determining landslide activity”. *International Journal of Remote Sensing*. 26(6), 1075-1092.

[10] Mondini, A.C., K. T. Chang, 2014. “Combining spectral and geoenvironmental information for probabilistic event landslide mapping”. *Geomorphology* 213, 183-189.

[11] Cheng, K., C. Wei, S. Chang, 2004. “Locating landslides using multi-temporal satellite images”. *Advances in Space Research* 33(3), 296-301.

[12] Carrara, A., 1993. “Uncertainty in evaluating landslide hazard and risk”. In: Nemeč J, Nigg JM, Siccardi F, editors. *Prediction and Perception of Natural Hazards: Proceedings Symposium, 22-26 October 1990, Perugia, Italy; Dordrecht. Springer Netherlands*. p. 101-109.

[13] Guzzetti, F., A. Carrara, M. Cardinali, P. Reichenbach, 1999. “Landslide hazard evaluation: a review of current techniques and their application in a multi-scale study, Central Italy”. *Geomorphology* 31, 181-216.

[14] Alvioli, M., I. Marchesini, P. Reichenbach, M. Rossi, F. Ardizzone, F. Fiorucci, F. Guzzetti, 2016. “Automatic delineation of geomorphological slope units with r.slopeunits v1.0 and their optimization for landslide susceptibility modeling”. *Geoscientific Model Development* 9, 3975-3991.

[15] Schlögel, R., I. Marchesini, M. Alvioli, M. Rossi, P. Reichenbach, J.-P., Malet, 2018. “Optimizing landslide susceptibility zonation: effects of DEM spatial resolution and slope unit delineation on logistic regression models”. *Geomorphology* 301, 10-20.

[16] Tucker, C.J., 1979. “Red and photographic infrared linear combinations for monitoring vegetation”. *Remote Sensing of Environment* 8(2), 127-150.

[17] Sohn, Y., N. Rebbello, 2002. “Supervised and unsupervised spectral angle classifiers”. *Photogrammetric Engineering and Remote Sensing* 68(12), 1271-1280.

[18] Richards, J., X. Jia, 2006. “Remote sensing digital image analysis”. Springer-Verlag Berlin Heidelberg, pp. 439

[19] Mondini, A.C., K. Tsung Chang, H. Yuan Yin, 2011. “Combining multiple change detection indices for mapping landslides triggered by typhoons”. *Geomorphology*.134(34), 440-451.

[20] Delon, J., A. Desolneux, J. L. Lisani, A. B. Petro, 2007. “A nonparametric approach for histogram segmentation”. *IEEE Transactions on Image Processing* 16(1), 253-261.

[21] Brakenridge, G., J. Syvitski, E. Niebuhr, I. Overeem, S. Higgins, A. Kettner, L. Prades, 2017. “Design with nature: causation and avoidance of catastrophic flooding, Myanmar”. *Earth-Science Reviews* 165(Supplement C), 81-109.

[22] Fiorucci, F., D. Giordan, M. Santangelo, F. Dutto, M. Rossi, F. Guzzetti, 2018. “Criteria for the optimal selection of remote sensing images to map event landslides”. *Natural Hazards and Earth System Sciences* 18, 405-417

[23] Mondini A. C., K. T. Chang, S. H. Chiang, R. Schlögel, C. Notarnicola, H. Saito, 2017. “Automatic mapping of event landslides at basin scale in Taiwan using a Monte Carlo approach and synthetic land cover fingerprints”. *Int J Appl Earth Obs Geoinf* 63(Supplement C), 112–121.

[24] Mondini, A.C., F. Guzzetti, P. Reichenbach, M. Rossi, M. Cardinali, F. Ardizzone, 2011. “Semiautomatic recognition and mapping of rainfall induced shallow landslides using optical satellite images”. *Remote Sensing of Environment* 115(7), 1743-1757.

[25] Blaschke, T., B. Feizizadeh, D. Hölbling, 2014. “Object-Based Image Analysis and Digital Terrain Analysis for Locating Landslides in the Urmia Lake Basin, Iran”. *IEEE J-STARS* 7(12), 4806-4817